Short-Time Dynamics of Partial Wetting

James C. Bird, Shreyas Mandre, and Howard A. Stone*

School of Engineering and Applied Sciences, Harvard University, Cambridge, Massachusetts 02138, USA

(Received 22 February 2008; published 11 June 2008)

When a liquid drop contacts a wettable surface, the liquid spreads over the solid to minimize the total surface energy. The first moments of spreading tend to be rapid. For example, a millimeter-sized water droplet will wet an area having the same diameter as the drop within a millisecond. For perfectly wetting systems, this spreading is inertially dominated. Here we identify that even in the presence of a contact line, the initial wetting is dominated by inertia rather than viscosity. We find that the spreading radius follows a power-law scaling in time where the exponent depends on the equilibrium contact angle. We propose a model, consistent with the experimental results, in which the surface spreading is regulated by the generation of capillary waves.

DOI: 10.1103/PhysRevLett.100.234501 PACS numbers: 47.55.nb, 47.55.df, 47.55.dr, 47.55.np

The spontaneous, capillary-driven spreading that results when a liquid drop contacts a solid surface forms the basis of many technological processes such as printing, coating, and adhesion [1]. Biological systems have also evolved to exploit spontaneous spreading; for instance, the secretion of a wetting liquid between the pretarsal pads of some insects helps them to adhere rapidly to surfaces [2,3]. Because of the ubiquity of spreading, it has been studied for over a century [4,5]. Yet, with the advent of ultrafast cameras, the first moments of spreading are now experimentally accessible [6–10], which is crucial to understanding rapid adhesion as it occurs in both technology and in nature.

When a drop contacts a perfectly wetting solid (equilibrium contact angle, $\theta_{eq} = 0°$), the initial dynamics are nearly identical to a drop coalescing with a wet film [9]. Such similarities between perfect wetting and coalescence are expected due to the presence of precursor films [5,9]. In both systems, spreading follows a power-law behavior that depends on the type of force resisting drop deformation. When inertia resists deformation, the spreading radius $r(t)$ scales as $(R\gamma/\rho)^{1/4}t^{1/2}$, where R is the drop radius, γ is the surface tension, ρ is the fluid density, and t is time [6,7,9,11]. On the other hand, in coalescence, when viscous effects resist deformation, the spreading radius changes according to $r(t) \propto \gamma t/\mu$, where μ is the dynamic viscosity of the drop, and there is a weak logarithmic dependence on time [8,11]. We are unaware of a study of the corresponding short-time viscous dynamics on a perfectly wetting surface.

Here, we focus on the early stages of partial wetting, $\theta_{eq} > 0°$, for which fundamental questions remain [12,13]. In this case, there are three different interfaces that intersect to form a contact line. When spreading occurs under partial wetting conditions, it is unknown whether the presence of a contact line prevents the occurrence of an inertial regime. Specifically, due to the divergence of viscous stresses at the contact line [14], viscous dissipation might be expected to be the dominant resistance to spreading. The only study that we have found that investigates early-time spreading on partially wetting surfaces does not address this issue [10]. The goal of this Letter is to investigate whether the inertial spreading observed for perfectly wetting fluids is also observed for the partial wetting regime. The observations that we report here show that the spreading dynamics for low equilibrium contact angles ($\theta_{eq} < 10°$) behaves similarly to that of a perfectly wetting fluid. However, for larger equilibrium contact angles, while the spreading is still regulated by inertia, the dynamics follow different power-law scalings which vary systematically with θ_{eq}.

The first step in our experiments was to prepare surfaces of variable wettability using a variety of coatings (Table I). Smooth silicon wafers were cleaned and coated following a standard silanization procedure [5]. Experiments were conducted for three deionized water-glycerol mixtures with volume proportions 100/0, 60/40, and 40/60. At 20 °C, the mixtures have reported viscosities of 1.0, 3.7, and 10.7 cP, respectively [15], which agreed with measurements we obtained using a double-Couette cell on a TA-ARG2 rheometer. The equilibrium

TABLE I. The equilibrium contact angle between the liquid, air, and substrate is modified by the type of silane used.

Surface	θ_{eq}	θ_{eq}	θ_{eq}
Wt. % glycerol	0	40	60
1. Thin liquid layer	0	0	0
2. Silicon dioxide	3	7	3
3. *N*-(3-triethoxysilypropyl)gluconamide	8	15	17
4. 3-Aminopropyltriethoxysilane	18	22	11
5. Acetoxyethyltriethoxysilane	38	37	32
6. Benzyltriethoxysilane	38	41	38
7. *n*-Octyltriethoxysilane	21	47	46
8. Triethoxysilybutraldehyde	43	44	47
9. (Heptadecafluoro-1,1,2,2-tetra-hydrodecyl)triethoxysilane	117	99	110
10. Soot	180	180	180

contact angles for these solutions with each substrate were measured from photographs and are reported in Table I.

For each trial, the appropriately coated silicon wafer is placed on a flat surface under a 600 μm diameter needle, through which liquid is injected quasistatically to create a nearly spherical drop (Fig. 1). Once the drop diameter equals the height of the needle, approximately 1 mm, the drop contacts the surface and spreads. The spreading dynamics are captured at 67 000 frames per second using a Phantom V7 camera. Image processing and the corresponding data analysis are accomplished using custom-made MATLAB algorithms. Contact ($t = 0$) corresponds to the frame before any visual changes are observed; this can occur a few frames before changes in the contact radius are measurable. Given the frame rate, our uncertainty in the start time is 15 μs for each trial.

The effect of surface chemistry on the shape of the drop as it spreads is shown in Fig. 1, which illustrates results for $\theta_{\mathrm{eq}} = 3°, 43°, 117°, 180°$. When a drop of water contacts the hydrophilic surface $\theta_{\mathrm{eq}} = 3°$ (Fig. 1 top row), the liquid near the surface spreads faster than that above it, and thus almost immediately an acute dynamic contact angle $\theta_D < 90°$ is formed. By contrast, when a drop of water contacts the hydrophobic surface ($\theta_{\mathrm{eq}} = 117°$ in Fig. 1), spreading occurs more slowly, and thus the drop maintains an obtuse dynamic contact angle, $\theta_D > 90°$, throughout the spreading. We note that there is a transition to $\theta_D = 90°$ when $\theta_{\mathrm{eq}} \approx 43°$ (Fig. 1, second row).

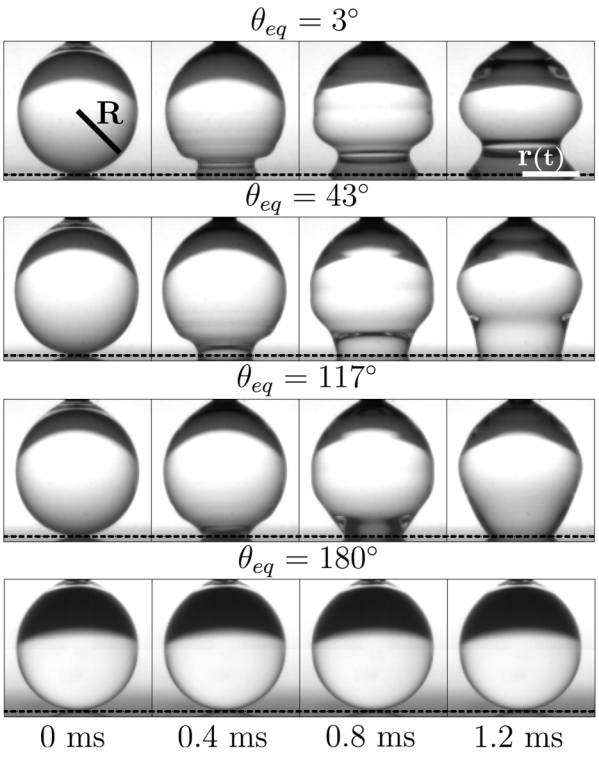

FIG. 1. When water drops (here, $R = 0.82 \pm 0.01$ mm) contact a surface (dotted line), the distance r that they spread during the first millisecond depends on the equilibrium contact angle θ_{eq} of the liquid on the surface. Here, water drops spread on surfaces 2, 8, 9, and 10 in Table I. It is clear that the surface chemistry has an effect on the drop shape during this spontaneous spreading.

In order to quantify the effects of wetting properties on the dynamics, we measured the spreading radius $r(t)$ during the initial stages of wetting for drops that ranged from 0.2–0.8 mm in radius. The results for drops on the four surfaces in Fig. 1 are shown in Fig. 2(a), which illustrates that drops spread faster on the hydrophilic surfaces than they do on the hydrophobic surfaces. We also observe that for each substrate, larger drops spread faster than smaller drops. By dimensional analysis, we know that in an inertially dominated case, $\frac{r}{R} = f(\frac{t}{\sqrt{\rho R^3/\gamma}}, \theta_{\mathrm{eq}})$, where $f()$ is some function. When our experimental data are nondimensionalized by this inertial scaling, all the trials collapse onto four master curves, one for each θ_{eq} [Fig. 2(b)]. If the dominant balance in the system was solely between capillarity and viscosity, then dimensional analysis predicts $\frac{r}{R} = f_1(\frac{t}{\mu R/\gamma}, \theta_{\mathrm{eq}})$. We confirmed that the viscous scaling does not provide any collapse of the data, and thus the collapse in Fig. 2 shows that the initial stages of wetting are inertially dominated.

A log-log plot of the same data reveals that the position of the contact line, $r(t)$, follows a power-law growth. Less significance should be placed on our data below dimensionless times of 0.1 due to the spatial accuracy of our measurements. Each of the curves in Fig. 3, corresponding to a distinct θ_{eq}, has a power-law exponent and prefactor, i.e., $r/R = C(t/\tau)^{\alpha}$ where $\tau \equiv \sqrt{\rho R^3/\gamma}$. We determined C and α for drops of three viscosities spreading on the ten different surfaces (see Table I) by fitting the data. The results are plotted in Fig. 4. As we now discuss, the effect of partial wetting is evident in the prefactor of the scaling law; more surprisingly, it also affects the exponent. We find that for low equilibrium contact angles, $\alpha \approx 1/2$, as was previously observed [9]. However, Fig. 3 demonstrates a monotonic decrease in the power-law exponent as the equilibrium contact angle increases. The coefficient C is of order one and also decreases for increasing contact angle. No visible spreading was observed on the soot surface ($\theta_{\mathrm{eq}} = 180°$), so the prefactor C was set to zero, and we were unable to report a value of α.

The power law $r/R = C(t/\tau)^{\alpha}$ can be written as $r = C(\gamma t/\rho)^{\alpha} R^{1-3\alpha/2}$. By varying t and R independently, we can obtain two independent measures of α. We carried out this secondary analysis for the three surfaces for which we varied the drop radius. The resulting points are reported in Fig. 4. Both approaches agree within experimental accuracy.

The log-log plot of the data for the spreading radius (Fig. 3) demonstrates two other points that we find noteworthy. First, we see a distinct change in exponent when the dimensionless time has a value between 2 and 3. This

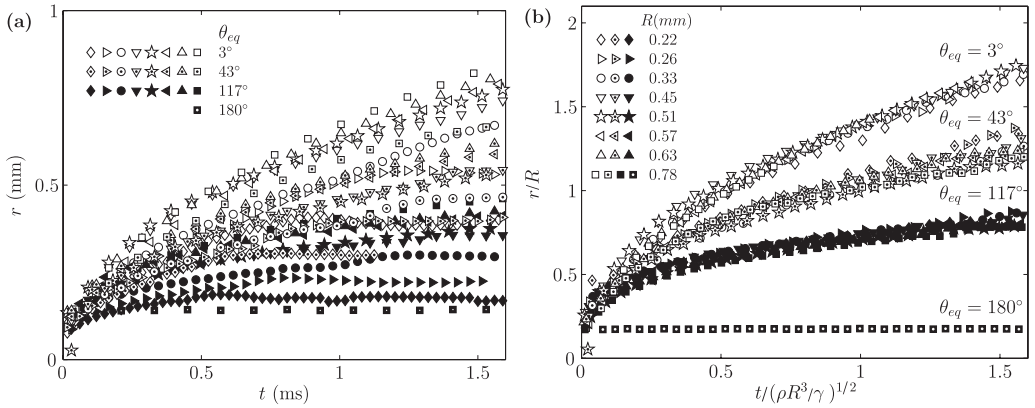

FIG. 2. Evidence of inertial wetting. (a) The spreading radius r is plotted at various times t for different sized drops (symbol shape) on each of the four surfaces in Fig. 1 (symbol shading). (b) Rescaling the plot by the drop radius R and a characteristic inertial time scale; the data collapses onto four master curves, each corresponding to a different equilibrium contact angle. A reduced data set is shown for clarity.

kink corresponds to the previously studied transition from inertial to viscous spreading [9]. Here, we observe that the time when this transition occurs is approximately independent of contact angle, and note that the inertial regime lasts for approximately as long as the capillary wave, generated at contact, takes to propagate over the drop. Surface tension will continue to drive spreading in the viscous regime until the drops reach their equilibrium shapes, which for the given contact angles (3°, 43°, 117°, 180°) correspond to spherical caps with radii $r/R \approx 33$, 2.4, 1.0, and 0, respectively. The second noteworthy feature of Fig. 3 is that the times at which the power-law responses commence appear to radiate from a single point. This observation suggests the possibility that either contact occurs at a finite radius [7] or that there is an even shorter time-spreading mechanism that does not depend on contact angle, e.g., [16]. Only after the spreading radius grows to about a tenth of the drop diameter do the effects of partial wetting begin to appear.

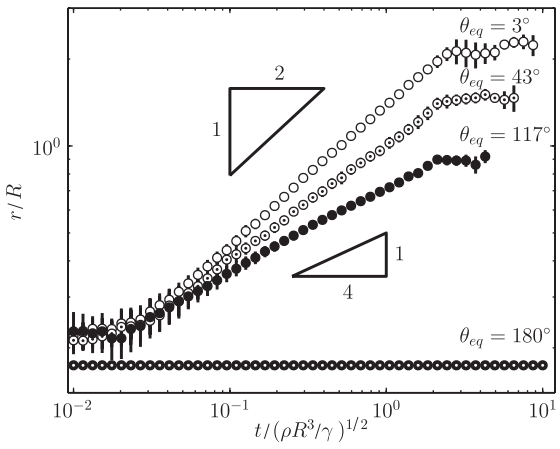

FIG. 3. Average of all trials for each of the four surfaces in Fig. 2. The normalized contact radius, r/R, shows a power-law spreading response where the exponent depends on the equilibrium contact angle θ_{eq}. The 95% confidence interval of the mean (two standard errors) is shown by the vertical lines. No error bars are depicted for $\theta_{eq} = 180°$ as only one trial was recorded.

The continuous dependence of the power-law exponent on the wetting properties (Fig. 4) is surprising. We are not able, at this time, to give a detailed analytical solution to this spreading problem; however, we propose a scaling analysis that can account for the contact angle-dependent spreading exponent.

Previous studies hypothesize that the early-time dynamics of inertial spreading is driven by an interface curvature proportional to R/r^2. When this curvature is regulated by the acceleration of liquid near the centerline of the drop, the resulting spreading radius scales as $t^{1/2}$ [6,7,9,11]. We are unable to modify this argument to account for the

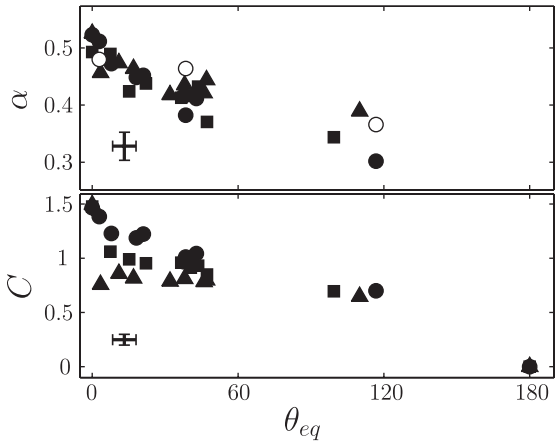

FIG. 4. The spreading dynamics can be fit to a power law, $r/R = C(t/\tau)^{\alpha}$. As the equilibrium contact angle, θ_{eq} increases, both the coefficient C and the exponent α decrease. The symbols represent the viscosity of the water-glycerol mixture—1.0 cP (●), 3.7 cP (■), and 10.7 cP (▲). The exponents derived using the secondary analysis described in the text (○) follow a similar trend. The uncertainly of when the drop contacts the substrate leads to an absolute error in the power-law exponents of approximately 5%.

partial wetting response (Fig. 1) and accommodate a contact angle-dependent exponent. An alternative approach is that spreading results from a rearrangement of liquid near the droplet surface with the motion in the interior playing a subdominant role. In other words, the generation and propagation of the capillary wave initiated at the contact line may be the rate limiting process. A two-dimensional planar version of these dynamics has been considered using potential flow theory [17] and leads to an exponent of $2/3$, irrespective of θ_{eq}. In fact, a number of theoretical studies in planar as well as axisymmetric geometries predict power-law exponents of $2/3$ for situations involving self-similar generation of capillary waves [17–19]. We postulate a different extension of these ideas to our experiments, which leads to a power law for the spreading radius with the exponent depending continuously on θ_{eq}.

To understand these ideas semi-quantitatively, consider the combined surface and kinetic energy, which is conserved in the absence of viscous dissipation,

$$\int_V \frac{1}{2}\rho|\mathbf{u}|^2 dV = \gamma[A(0) - A(t) + \pi r(t)^2 \cos\theta_{eq}]. \quad (1)$$

Here, $\mathbf{u}(\mathbf{x}, t)$ is the velocity field as a function of position $\mathbf{x}$ and time, and $A(t)$ is the surface area of the liquid-vapor interface. Immediately after contact, we expect self-similar dynamics to ensue [17], justifying the power-law behavior. By estimating the magnitudes of the two sides of (1), we extract the power law.

The images of the drop spreading in Fig. 1 suggest that the region of deformation grows at the speed of capillary waves. We assume a self-similar velocity field to vary over the length $\ell_{ci} \propto (\gamma t^2/\rho)^{1/3}$ [17], near the contact line, with the magnitude of the velocity field determined by the contact line speed $u \propto dr/dt$. We also expect that the amplitude of the traveling wave to scale as the spreading radius, r. As a result, the change in the surface area of the spreading drop scales as r^2, i.e., $A(0) - A(t) = \pi F(\theta_{eq}) r(t)^2$, for some undetermined function F.

Substituting into (1), we find that the spreading radius satisfies the equidimensional equation

$$\frac{t}{r}\frac{dr}{dt} \propto \sqrt{F(\theta_{eq}) + \cos\theta_{eq}}. \quad (2)$$

The nondimensionalized solution to this equation is $r/R = C(t/\tau)^{\alpha}$ where $\alpha = C_1\sqrt{F(\theta_{eq}) + \cos\theta_{eq}}$, C_1 being a proportionality constant in (2). Thus, consistent with the experimental observations, the scaling exponent, α, depends only on the equilibrium contact angle, but not on any other physical parameters. Additionally, this exponent predicts the basic trend in the data (Fig. 4) provided that the unknown function F only weakly depends on θ_{eq}. For $\theta_{eq} = 0$, we find no predisposition for or against the observed value $\alpha \approx 1/2$. A resolution of this issue requires a more detailed theory.

In summary, we find that early-time inertially dominated wetting extends beyond perfectly wetting situations and into the spreading of partially wetting fluids. The experiments clearly demonstrate that the surface chemistry and size of the drop are important in the initial spreading dynamics, whereas the fluid viscosity is not. The spreading rate exhibits a power-law-like behavior whose exponent depends on the equilibrium contact angle. Similar results were also obtained when a silanized glass slide was substituted for the silicon wafer. While we currently lack a detailed theory to rationalize these results, we have offered an explanation at the level of a scaling law, with the important idea being the propagation of capillary waves. This finding is relevant to biological and nonbiological coating processes, particularly in determining initial transients in rapid adhesion.

We thank L. Courbin and A. Ajdari for helpful discussions and J. Wan and C. Osuji for assistance in surface preparation and rheological measurements, respectively. We also thank the NSF via the Harvard MRSEC (No. DMR-0213805) and IGERT programs for support of this research.

*has@deas.harvard.edu

[1] E. Cohen and E. Gutoff, *Modern Coating and Drying Technology* (John Wiley and Sons, Inc., New York, 1992).
[2] H. F. Bohn and W. Federle, Proc. Natl. Acad. Sci. U.S.A. **101**, 14138 (2004).
[3] J. Qian and H. J. Gao, Acta Biomaterialia **2**, 51 (2006).
[4] P. G. de Gennes, Rev. Mod. Phys. **57**, 827 (1985).
[5] P. G. de Gennes, F. Brochard-Wyart, and D. Quere, *Capillarity and Wetting Phenomena* (Springer, New York, 2004).
[6] M. M. Wu, T. Cubaud, and C. M. Ho, Phys. Fluids **16**, L51 (2004).
[7] S. T. Thoroddsen, K. Takehara, and T. G. Etoh, J. Fluid Mech. **527**, 85 (2005).
[8] D. G. A. L. Aarts, H. N. W. Lekkerkerker, H. Guo, G. H. Wegdam, and D. Bonn, Phys. Rev. Lett. **95**, 164503 (2005).
[9] A. L. Biance, C. Clanet, and D. Quere, Phys. Rev. E **69**, 016301 (2004).
[10] J. Drelich and D. Chibowska, Langmuir **21**, 7733 (2005).
[11] J. Eggers, J. R. Lister, and H. A. Stone, J. Fluid Mech. **401**, 293 (1999).
[12] J. Eggers, Phys. Rev. E **72**, 061605 (2005).
[13] C. Duez, C. Ybert, C. Clanet, and L. Bocquet, Nature Phys. **3**, 180 (2007).
[14] C. Huh and L. E. Scriven, J. Colloid Interface Sci. **35**, 85 (1971).
[15] *CRC Handbook of Chemistry and Physics, Internet Version 2007*, edited by D. R. Lide (Taylor and Francis, Boca Raton, FL, 2007), 87th ed..
[16] S. C. Case and S. R. Nagel, Phys. Rev. Lett. **100**, 084503 (2008).
[17] J. B. Keller, P. A. Milewski, and J. M. Vanden-Broeck, Eur. J. Mech. B, Fluids **19**, 491 (2000).
[18] J. Billingham and A. C. King, J. Fluid Mech. **533**, 193 (2005).
[19] S. P. Decent and A. C. King, IMA J. Appl. Math. **73**, 37 (2007).